Nano-structure solar cells on the base of p-Si/$Cd_{1-x}Zn_xO$ thin film heterojunctions

H. M. MAMEDOV*, V. U. MAMMADOV, V. J. MAMMADOVA, Kh. M. AHMEDOVA, E. B. TAGIYEV, L. E. AGAZADE

Faculty of Physics, Department of Physical Electronics, Baku State University, Az1148, Z.Khalilov str., 23, Baku, Azerbaijan, e-mail: mhhuseyng@bsu.edu.az; mhhuseyng@gmail.com

In this paper heterojunctions of p-Si/$Cd_{1-x}Zn_xO$ were deposited by the method of electrochemical deposition. The electric and photoelectrical properties of p-Si/$Cd_{1-x}Zn_xO$ heterojunctions, surface morphology and optical properties of $Cd_{1-x}Zn_xO$ films were investigated depending on the electrochemical deposition potential and films composition. It is found out that heterojunctions of p-Si/$Cd_{1-x}Zn_xO$ with nano-structured surface, which deposited at cathode potential of -1.2 V, shows good rectification (k≈640). Under AM1.5 conditions (W = 100 mW/cm^2) the maximal values of open-circuit voltage, short-circuit current, fill factor and efficiency of our best nano-structured cell, were U_{oc} = 442 mV, J_{sc} = 12.9 mA/cm^2, FF = 0.57 and η = 3.25 %, respectively.

(Received May 11, 2018; accepted October 10, 2018)

Keywords: Electrochemical deposition, Thin film, Heterojunction, Solar cell

1. Introduction

Thin films of ZnO are one of the favorable materials for the production of opto- and photoelectronic devices [1-3]. CdO films is conducting, transparent in the visible region with a direct band gap of 2.5 eV and which useful for as solar cells, gas sensors, windows, and thin-film resistors [4-6], and most importantly, shows low resistance. Therefore, the resistivity of ZnO can be decrease by alloying with CdO. Creation of solid solutions on the basis of various metal oxides and chalcogenides allows changing physical properties and band gap of thin films that is actual at designing of photonic devices with high performance in various spectral ranges [7-13]. A variety of methods have been reported for the preparation of CdO–ZnO alloy films such as molecular beam epitaxy [14], sol–gel process [15] and spray pyrolysis [16]. Among these methods, electrodeposition is an attractive method to obtain these kinds of films [17-19], which is well known for its simplicity, reproducibility and possibility of producing cheap large-area films [9-13]. Although pure ZnO and CdO films have been studied by many research groups, a compound semiconductor of ZnO and CdO, that is to say, $Cd_{1-x}Zn_xO$ has seldom been studied.

In this work, we present electrical and photoelectrical properties of p-Si/$Cd_{1-x}Zn_xO$ (with x=0.4; 0.5; 0.6; 0.7; 0.8 and 0.9) heterojunctions deposited by electrodeposition method onto the *glass*/Al/p-Si as substrates.

2. Experiment

The electrochemical deposition of $Cd_{1-x}Zn_xO$ films has been performed with a three electrode configuration: graphite electrode as anode, Ag/$AgCl_3$ electrode as reference electrode and vacuum evaporated p-Si thin films (2.5 Ω·cm resistivity and 200 μm thickness) onto the *glass*/Al substrates as cathode. For SEM, energy dispersive spectra (EDS), electrical and optical measurements we used the *glass*/SnO_2 substrates. Total area of working electrodes (cathode) was 1×1 cm^2. The *glass*/Al/p-Si substrates were cleaned with ethanol, acetone and deionized water and then dried in flowing N_2. At electrodeposition we used aqueous solutions of $Zn(NO_3)_2$ and $Cd(NO_3)_2$ salts (99.5% purities) with different molar fraction in solution (Table 1). The solution were kept on continuous stirring for 1 hour then filtered by filter paper. The solution was homogeneous, clear, transparent and stable at room temperature. The reaction temperature was kept at 80°C. In order to investigate the electrochemistry in the deposition process of $Cd_{1-x}Zn_xO$, cyclic voltammetry study was performed in the potential range of -1.6 to +1.6 V. $Cd_{1-x}Zn_xO$ formation potentials region were registered from cyclic voltammetry curves, and are summarized in Table 1.

Table 1. Mole fraction of salts, deposition current and potential for the $Cd_{1-x}Zn_xO$ films

x	Mole fraction of salts (mM)		Deposition current and potential	
	$Zn(NO_3)_2$	$Cd(NO_3)_2$	J, mA/cm^2	U_c (V)
0.2	1.22	4.88	5.6	-0.96 – -1.21
0.4	4.13	6.21	5.1	-0.96 – -1.24
0.5	4.91	4.94	4.2	-0.93 – -1.26
0.6	5.92	3.95	3.4	-0.88 – -1.37
0.7	6.34	2.73	3.2	-0.89 – -1.38
0.8	6.5	1.63	2.7	-0.9 – -1.37
0.9	6.85	0.76	2.4	-0.91– -1.38

The thickness of $Cd_{1-x}Zn_xO$ films were about 100 – 500 nm, depending on the deposition duration. All the films showed n-type conductivity. Hall Effect measurements showed that the resistivity of films was 2×10^{-3} – 170 Ω·cm and the free electron concentration was $n = 6.5\times10^{17} – 8\times10^{14}$ cm^{-3}, depending on the Zn content.

EDS data were recorded to determine the composition of Cd and Zn in deposited layers. The stoichiometries ratio of Zn and Cd are displayed in Fig. 1.

In order to fabricate the heterojunctions, an Ohmic In (or Au) electrode, in reticulose form was evaporated on the $Cd_{1-x}Zn_xO$ films with an area of ~0.62 cm^2. Aluminum (Al) was evaporated on the back side of the *p*-Si wafer as the Ohmic electrode, followed by annealing at 500°C in vacuum for 20 min.

3. Results and discussions

It is established that morphology of $Cd_{1-x}Zn_xO$ films depends on the deposition potential. SEM images of films $Cd_{0.4}Zn_{0.6}O$ deposited at -0.9V, -1.2V, -1.28 V and -1.35 V are shown in Fig. 2. The morphology of films deposited at -0.9 V are homogeneous micro-texture structure (Fig. 2a). The SEM images showed that the size of the crystallites decreased with increasing deposition potential from -0.9 V to -1.2 V and films demonstrate nanostructure surface (Fig. 2b).

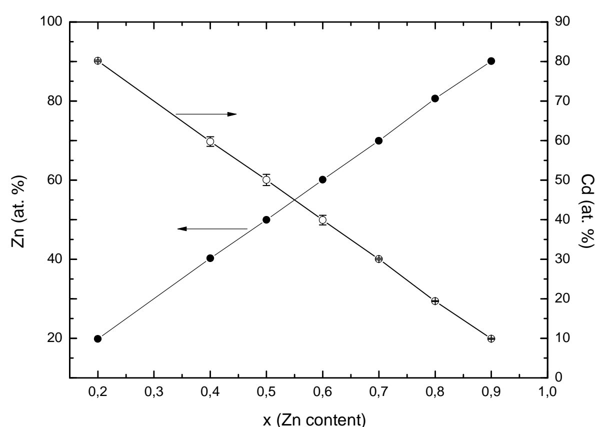

Fig. 1. Atomic percentage of Zn and Cd in the $Cd_{1-x}Zn_xO$ thin films with thickness of 500 nm (deposited at -1.2 V) recorded by EDS measurements at room temperature

The particle sizes and shape distribution looks more uniform compared to films deposited at other potentials. The uniformity in particles shape is due to higher nucleation rate and uniform particle growth. The concentration of surface defects increases by increasing the deposition potential from -1.28 to -1.32 V (Fig. 2c). Future growth of the potential (U>-1.34V) leads to increase of non-homogeneity degree at surface and films shows poor adhesion to surface (Fig. 2d).

$Cd_{1-x}Zn_xO$ thin films deposited on *glass*/SnO_2 substrates show high transmission in the visible and UV range with average transmission ranging between 52-93% with variation of cathode potential, showing that films can be used as transparent window materials in many opto- and photo- electronic devices. As seen from Fig. 3, films deposited at -0.9V shows not sharp and complicated absorption edge in the short wavelength range. It shows that films deposited at -0.9 V contains not one, and a few crystal phases (segregation of the phases) [20]. Higher transmission value (93%) was observed for samples prepared at -1.2V. The linear dependence of $(\alpha h\nu)^2$ to $h\nu$ indicates that $Cd_{0.4}Zn_{0.6}O$ films are direct transition type semiconductors. Films deposited at -1.35 V shows again complicated absorption edge and little transmittance (65%) because of crystal phase segregations or high scattering in the films.

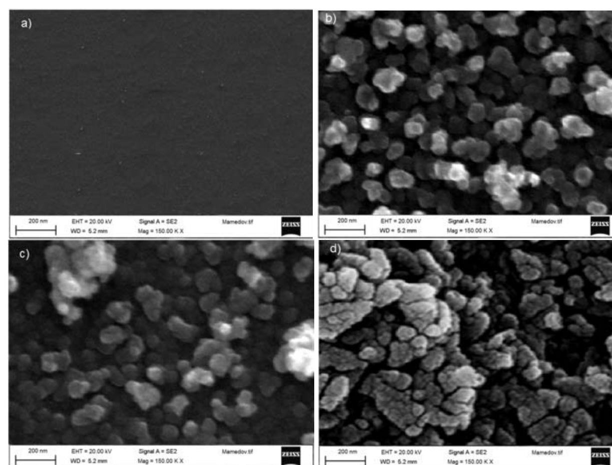

Fig. 2. SEM images of films $Cd_{0.4}Zn_{0.6}O$ deposited at -0.9V (a), -1.2V (b), -1.28 V (c) and -1.35 V (d)

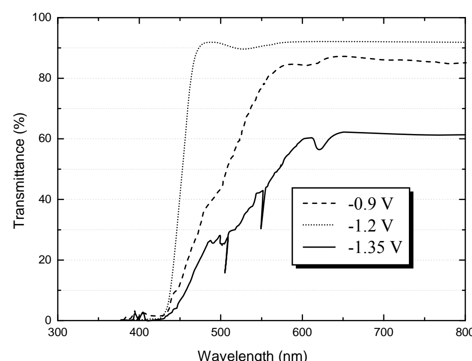

Fig. 3. Optical transmittance spectrum of films $Cd_{0.4}Zn_{0.6}O$ deposited at different potentials

The band gap of the $Cd_{1-x}Zn_xO$ films deposited at -1.2V were determined from extrapolation of the straight line section of the $(\alpha h\nu)^2$ versus $h\nu$ curves (Table 2). The bandgap calculated above has been found to decrease linearly from 2.95 eV (x = 0.6) to 2.64 eV (x = 0.2) as a function of Zn concentration. The calculated values of the band gap are found in good agreement with the values of band gap reported in [7, 20].

Table 2. Bandgap of films $Cd_{1-x}Zn_xO$ with different Zn content

$Cd_{1-x}Zn_xO$ (x)	Bandgap (eV)
0.2	2.64
0.4	2.82
0.5	2.91
0.6	2.95
0.7	3.04
0.8	3.14
0.9	3.22

Electrical and photoelectrical properties of heterojunctions were studied depending on the on the deposition potential and Zn content.

Current-voltage characteristics (J-V) of heterojunctions deposited at -0.9V, -1.2V, -1.28 V and -1.35 V show rectification. It is established that rectification factor values on the deposition potential (Fig. 4). The pass direction corresponds to positive polarity of the external bias on the p-Si layers. As seen from figure 4, the rectification increases from 32 up to 640, with increasing the deposition potential from -0.9V to -1.2V. Further increase in deposition potential leads to sharp decrease of rectification (~10÷12).

The experimental J-V curves, measured at 300 K, for p-Si/$Cd_{1-x}Zn_xO$ heterojunction using various values of x are illustrated in Fig. 5. These curves were definitely of the diode type, with the forward direction corresponding to the positive potential on p-Si. Built-in potential (V_{bi}), series resistance (R_s), ideality factor (n) and rectification factor (k) of heterojunctions depending on the Zn content were determined from J-V curves and summarized in Table 3.

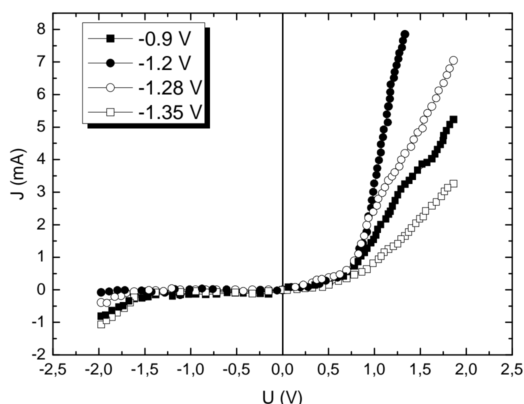

Fig. 4. Dark J-V characteristics of p-Si/$Cd_{0.4}Zn_{0.6}O$ heterojunctions deposited at different cathode potential

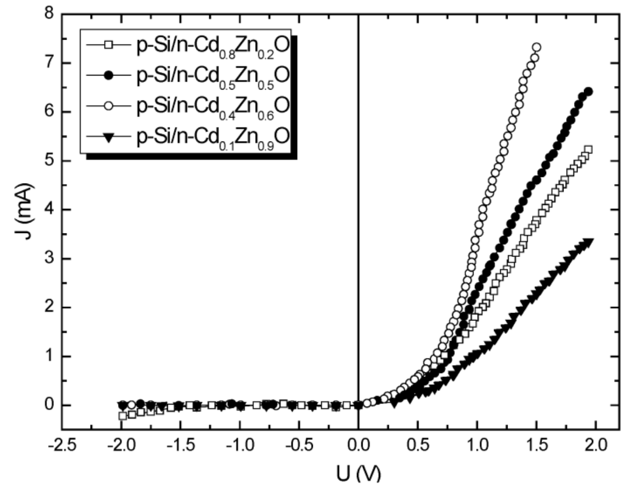

Fig. 5. Dark J-V characteristics of p-Si/$Cd_{1-x}Zn_xO$ heterojunctions with different Zn content.

As seen from the Fig. 5 and Table 3, the series resistance of heterojunctions increases with Zn content, which is due to the increase of $Cd_{1-x}Zn_xO$ films resistance. However, there is non-linear dependence of rectification coefficient and ideality factor on the Zn content.

The minimum value of ideality factor is observed in heterojunctions with x=0.6 (Table 3), that show close lattice constants of the Si and $Cd_{0.4}Zn_{0.6}O$. Thus, according to Fig. 4, the rectification in junctions with x=0.6 reaches value of k=640 at ±1.5V (Table 3). It must be noted that, rectification in heterojunctions on the basis of $Cd_{1-x}Zn_xO$ for all Zn content is much larger than that reported for p-Si/ZnO [21-23].

C–V characteristics at different frequencies and forward J-V characteristics of structures in log scale at various temperatures and Zn content were investigated to explain the mechanism of current passage through junctions.

Table 3. Electrical parameteres of heterojunctionsp-Si/$Cd_{1-x}Zn_xO$ deposited at -1.2 V, depending on the Zn content

Samples x	n	V_{bi} (V)	V_c (V)	R_s (kΩ)	k
0.2	2.4	0.44	0.48	0.01	190
0.4	2.1	0.49	0.51	0.03	246
0.5	1.79	0.56	0.52	0.05	583
0.6	1.74	0.56	0.55	0.07	640
0.7	1.96	0.56	0.57	2	480
0.9	2.63	0.59	0.62	40	235

The forward current of heterojunctions with x≠ 0.6, is significantly dependent on the Zn content (Fig. 6). The J-V plots of these junctions reveal two regions, having two different slopes, which sharply depend on the temperature (not shown here).

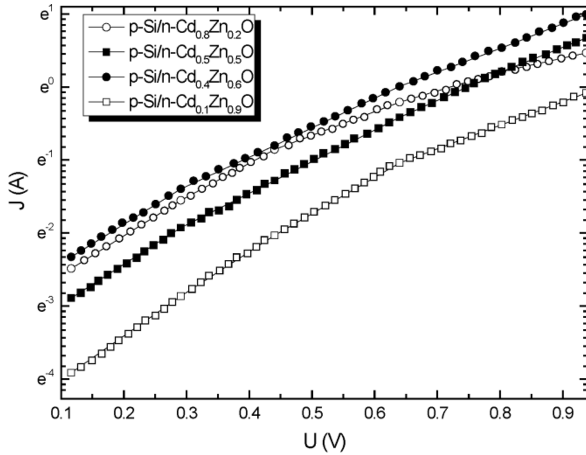

Fig. 6. Semilogarthmic plots of forward dark J-V characteristics of the p-Si/$Cd_{1-x}Zn_xO$ heterojunctions with different Zn content

It should be noted that the *C–V* characteristics of junctions with $x \neq 0.6$ have peculiarities, typical for heterojunctions with the presence of defects at the junction region. Since, the *C–V* characteristics of these junctions are poorly linearized in $C^{-2}(V)$ coordinates and its slope changes by frequency of the alternating signal (Fig. 7). In addition, the value of cut-off voltage (V_c) determined from *C–V* characteristics is less in comparison with built-in potential (V_{bi}), determined from the linear section of *J-V* curves measured at room temperature (Table 3). The observed effect in heterojunctions can be explained by the dependence of relaxation times of surface states on the frequency of the alternating signal [24, 25].

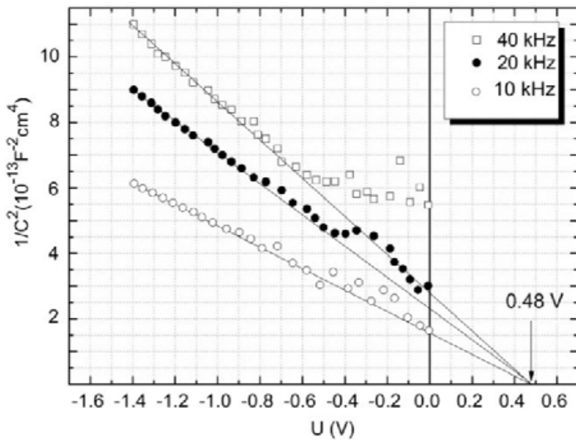

Fig. 7. C-V characteristics of p-Si/$Cd_{0.8}Zn_{0.2}O$ heterojunctions deposited at different potentials

However, *J-V* plots of junctions with x=0.6, reveal only one region. It is established, that the linear region of the dependence $lnI = f(V)$ do not depend on temperature which indicates the possibility of the tunneling mechanism of current passage (Fig. 8). However, at low applied voltages the space-charge region is not thin enough for direct tunneling. The concentration of surface states, associated with lattice mismatch between the Si and $Cd_{0.4}Zn_{0.6}O$, were calculated using the method described in [26], which is about $n \approx 6\times10^{13}$ cm^{-3}. Therefore, it is possible to consider multistage tunnel-recombination mechanism of current passage, with participation of surface states at interface.

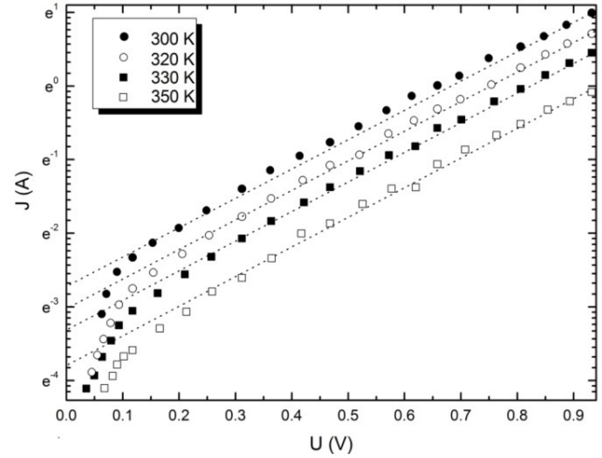

Fig. 8. Semilogarthmic plots of forward dark J-V characteristics of the p-Si/$Cd_{0.4}Zn_{0.6}O$ heterojunctions at different temperatures

C–V characteristics of these junctions are linearized in $C^{-2}(V)$ coordinates and there is weak dependence of slope on the AC signal frequency, which indicates the low concentration of surface states, in comparison with heterojunctions with $x \neq 0.6$ (Fig. 9). The linearity of *C–V* characteristics in $C^{-2}(V)$ coordinates indicates a sharp distribution of uncompensated acceptor impurities, showing that the investigated heterojunctions are abrupt.

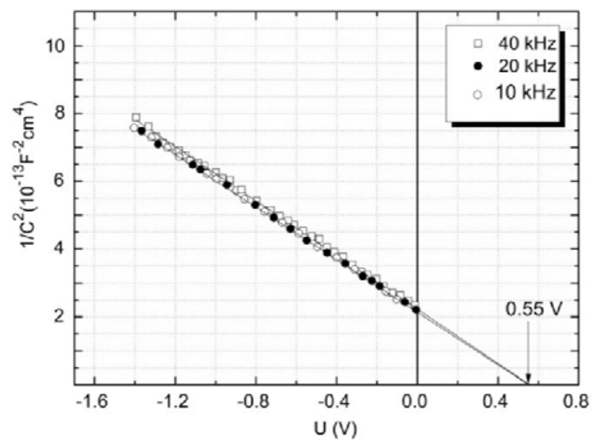

Fig. 9. C-V characteristics of p-Si/$Cd_{0.4}Zn_{0.6}O$ heterojunctions at different AC signal frequency

Under standard test conditions (W=100 mW/cm^2), all investigated heterojunctions demonstrated photovoltaic performances, which sign of open circuit photo-voltage (U_{oc}) does not change in all region of photosensitivity. However, the maximum values of U_{oc} and J_{sc} non-monotonically dependent on the Zn content and deposition potential. The maximum values of U_{oc} and J_{sc} were observed for heterojunctions with x=0.6 deposited at -1.2V (Fig. 10 and Table 4).

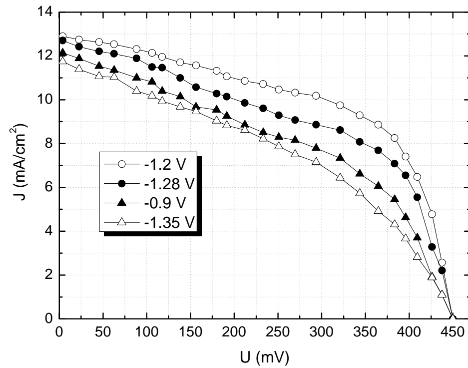

Fig. 10. Light (W=100 mW/cm^2) J-V characteristics of p-Si/$Cd_{0.4}Zn_{0.6}O$ heterojunctions deposited at different cathode potential

Table 4. Photoelectrical parameteres of heterojunctions p-Si/$Cd_{1-x}Zn_xO$ deposited at -1.2 V, depending on the Zn content

Samples x	U_{oc} (mV)	J_{sc} (mA/cm^2)	FF	η, %
0.2	162	14.4	0.44	1.03
0.4	263	13.8	0.51	1.85
0.5	403	13.2	0.51	2.71
0.6	442	12.9	0.57	3.25
0.7	380	8.4	0.48	1.53
0.9	320	6.8	0.45	0.98

We investigated the spectral distribution of photocurrent (J_{ph}) depending on the Zn content, in wavelength range of 200÷1300 nm (Fig. 11). The near infrared photosensitivity falloff for all heterojunctions indicated Si absorber band gaps of 1125 nm. A drastically different spectral response is observed under illumination of the heterojunctions from the other side, which gives rise to a short wavelength peak in the spectral dependence of the photocurrent. With increasing x, the short wavelength peak shifts to shorter wavelengths, which is attribute to the increase in the band gap of $Cd_{1-x}Zn_xO$ and intensity of peaks decrease with x. At x = 0.6, the peak is observed at 420 nm (Fig. 11).

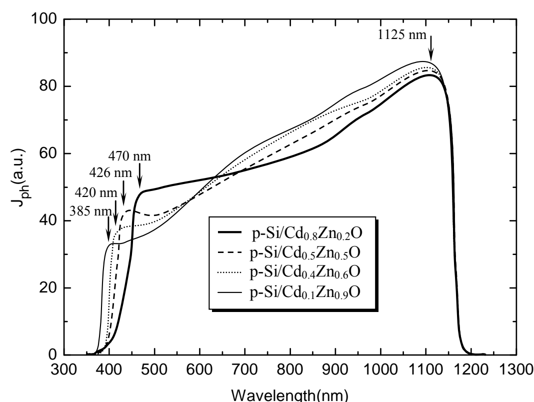

Fig. 11. Spectral distribution of photocurrent for heterojunctions p-Si/$Cd_{1-x}Zn_xO$ with different Zn content

4. Conclusion

Thus, electrical and photoelectrical parameters of heterojunctions p-Si/$Cd_{1-x}Zn_xO$ can be controlled by $Cd_{1-x}Zn_xO$ films composition and deposition potential. Heterojunctions with x=0.6, deposited at -1.2 V with nano-structured surface shows best photoelectric parameters: under AM1.5 conditions the maximal values of open-circuit voltage, short-circuit current, fill factor and efficiency of our best cell, were U_{oc} = 442 mV, J_{sc} = 12.9 mA/cm^2, FF = 0.57 and η = 3.25 %, respectively.

References

[1] X. Li, X. Xu, Z. Quan, J. Guo, H. Wu, G. A. Gehring, J. Appl. Phys. **105**, 103914 (2009).
[2] X. Han, K. Han and M. Tao, ECS Trans. **25**, 93 (2010).
[3] W. Liu, F. Xiu, K. Sun, Y. Xie, K. L. Wang, Y. Wang, J. Zou, Z. Yang and J. Liu, J. Am. Chem. Soc. **132**, 2498 (2010).
[4] R. A. Ismail, O. A. Abdulrazaq, Sol. Energy Mater. Sol. Cells **91,** 903 (2007).
[5] R. S. Mane, H. M. Pathan, C. D. Lokhande, S. H. Han, Sol. Energy **80**, 185 (2006).
[6] E. Martin, M. Yan, M. Lane, J. Ireland, C. Kannewurf, R. H. Chang, Thin Solid Films **461**, 309 (2004).
[7] Y. Caglar, M. Caglar, S. Ilican, A. Ates, J. Phys. D: Appl. Phys. **42**, 065421 (2009).
[8] F. Wang, Z. Ye, D. Ma, L. Zhu, F. Zhuge, J. Cryst. Growth **283**, 373 (2005).
[9] A. Abdinov, H. Mamedov, S. Amirova, Jpn. J. Appl. Phys. **46**, 7359 (2007).
[10] A. Abdinov, H. Mamedov, H. Hasanov, S. Amirova, Thin Solid Films **480-481**, 388 (2005).
[11] A. Abdinov, H. Mamedov, S. Amirova, Thin Solid Films **511-512**, 140 (2006)
[12] H. Mamedov, V. Mamedov, V. Mamedova, K. Ahmadova, J. Optoelectron. Adv. M. **17**(1-2), 67 (2015).
[13] H. Mamedov, Z. Konya, M. Muradov, A. Kukovecz, K. Kordas, D. Hashim, V. Mamedov, J. Solar Energy Engineering **136**, 044503 (2014).
[14] S. Sadofev, S. Blumstengel, J. Cui, J. Puls, S. Rogaschewski, P. Schafer, F. Henneberger, Appl. Phys. Lett. **89**, 201907 (2006).
[15] G. Torres-Delgado, C.I. Zuniga-Romero, O. Jimenez-Sandoval, R. Castanedo-Perez, B. Chao, S. Jimenez-Sandoval, Adv. Funct. Mater. **12**, 129 (2002).
[16] H. Tabet-Derraz, N. Benramdane, D. Nacer, A. Bouzidi and M. Medles, Sol. Energy Mater. Sol. Cells **73,** 249 (2002).
[17] M. Tortosa, M. Mollar, B. Marı, J. Cryst. Growth **304**, 97 (2007).
[18] Trilok Singh, R. Singh, Journal of Alloys and Compounds **509**, 5095 (2011).
[19] Trilok Singh, R. Singh, Journal of Alloys and

Compounds **552**, 294 (2013).
[20] A. Singh, D. Kumar, P. K. Khanna, M. Kumar, B. Prasad, ECS Journal of Solid State Science and Technology **2**(9), Q136 (2013).
[21] F. Z. Bedia, A. Bedia, B. Benyoucef, S. Hamzaoui, Physics Procedia **55**, 61 (2014).
[22] M. Jing-Jing, J. Ke-Xin, L. Bing-Cheng , F. Fei, X. Hu, Z. Chao-Chao, C. Chang-Le, Chin. Phys. Lett. **27**(10), 107304 (2010).
[23] T. Xiao-Yun, W. Yan-Hua, Y. Wei, G. Wei, F. Guang-Sheng, Chin. Phys. B **21**(9), 097105 (2012).
[24] I. Balberg, J. Appl. Phys. **58**, 2603 (1985).
[25] P. Chattopadhyay, D. P. Haldar, Appl. Surf. Sci. **171**, 207 (2001).
[26] V. P. Makhniy, S. V. Khusnutdinov, V. V. Gorley. Acta Phys. Polon. A **116**, 859 (2009).

*Corresponding author: mhhuseyng@bsu.edu.az
mhhuseyng@gmail.com